Coupled 3D Mechano-Electrochemical Finite Element Modeling of Interacting Corrosion Defects in Buried Pipelines

Umair Sarwar
Department of Mechanical Engineering, Universiti Teknologi PETRONAS, Malaysia
umair_22001647@utp.edu.my (corresponding author)

Ainul Akmar Mokhtar
Department of Mechanical Engineering, Universiti Teknologi PETRONAS, Malaysia
ainulakmar_mokhtar@utp.edu.my

Hilmi Hussin
Department of Mechanical Engineering, Universiti Teknologi PETRONAS, Malaysia
hilmi_hussin@utp.edu.my

Masdi Muhammad
Department of Mechanical Engineering, Universiti Teknologi PETRONAS, Malaysia
masdimuhammad@utp.edu.my

Afzal Ahmed Soomro
Interdisciplinary Research Center for Industrial Nuclear Energy, KFUPM, Dhahran, Saudi Arabia
afzals.09in09.muet@gmail.com

Nadir Hussain
Nano Fusion Technology Research Group, Division of Frontier Fibers, Institute for Fiber Engineering, Interdisciplinary Cluster for Cutting Edge Research, Shinshu University, Japan
engr.nadir712@hotmail.com

Received: 30 October 2025 | Revised: 17 November 2025 | Accepted: 21 November 2025

 DOI: https://doi.org/10.48084/etasr.15881

ABSTRACT

Buried pipelines face significant challenges from external corrosion, particularly stress corrosion. This localized form of degradation is driven by the influence of mechanical stresses, soil environments, and electrochemical reactions. This study developed a Three-Dimensional (3D) Finite Element (FE) model to analyze the Mechano-Electrochemical (M-E) effects on corroded pipelines. Understanding the effects of M-E interaction in corrosion processes is crucial for ensuring the integrity and longevity of these pipelines. The study presents a 3D FE simulation using COMSOL Multiphysics software to investigate the M-E effect on corrosion defects by simulating the stress corrosion behavior of X46 buried steel pipeline. The results reveal that increasing longitudinal tensile strain and corrosion defect depth lead to localized stress enhancements on the pipe wall. While tensile strain leads to an increase in the overall stress level, deeper corrosion defects concentrate stress at the defect center.

Keywords-mechano-electrochemical; 3D FE model; stress corrosion; buried pipelines; corrosion defects

I. INTRODUCTION

Despite the high structural integrity of current pipelines, they experience various types of corrosion due to the harsh operating environment [1-3]. Pipeline corrosion can cause wall thinning, perforations, or rupture, increasing the risk of fires, explosions, and compromising human safety and infrastructure integrity. Furthermore, leakage of hydrocarbons can severely contaminate soil and water, damaging ecosystems and compromising biodiversity [4-6]. Approximately 40% of the documented pipeline incidents and failures worldwide are directly attributed to corrosion-related damage [2]. Buried oil and gas pipelines are particularly vulnerable to corrosion due to prolonged exposure to aggressive soil environments, groundwater, microbial activity, and fluctuating operating conditions [7, 8]. External corrosion not only endangers human life and the environment but also results in substantial economic losses and disruption of energy supply. Therefore, accurate identification and prediction of external corrosion are significant for ensuring the integrity of buried oil and gas pipeline systems.

For buried oil and gas pipelines, stress corrosion is a crucial issue [9], with documented cases across major producing nations including the United States, Canada, Russia, Australia, Saudi Arabia, and Iran. The complexity of stress corrosion in pipelines stems from its dependence on multiple interacting factors. Steel pipelines are subjected to complex stress and strain conditions, including hoop stress from operating pressure and soil stress from ground movement [10]. The complex interplay between mechanical stresses and electrochemical reactions at corrosion defect sites creates a synergistic effect, known as the M-E effect [11, 12]. The M-E effect plays a substantial role in stress corrosion by accelerating electrochemical reactions under mechanical action [13, 14]. Authors in [11, 15-18] investigated the M-E effect in corroded pipe defects under near-neutral pH bicarbonate (NS4) solution. Their findings demonstrate the significant influence of the tensile stress and corrosion depth on the M-E effect at the defect site.

Authors in [19, 20] developed an FE model incorporating the M-E effect to analyze the growth of corrosion defects on X100 pipeline steel. Their findings revealed distinct growth rates across defect dimensions, with depth progression occurring most rapidly, followed by length and width extension. Similarly, authors in [21] designed a 3D FE model to examine the M-E effect, indicating stress concentration at the defect center with increasing strain and corrosion depth. Authors in [22] applied the FE method to simulate corrosion pits using the M-E effect, demonstrating interaction between stress concentration and pit depth. Previous studies have mostly applied simple 2D models, which fail to analyze the intricacies of stress corrosion, and 3D models with a single corrosion defect. Therefore, the present study developed a 3D FE model to examine the M-E effect at two external corrosion defects. The model employs computational methodologies, including the advancement of complex boundary conditions, high-quality mesh generation, and parameter specification to achieve highly reliable simulation outcomes.

II. FINITE ELEMENT MODELING

A. *Geometry Model and Boundary Conditions*

The FE model was developed using COMSOL Multiphysics software to simulate the complex interactions of mechanical stresses, electrochemical reactions, and their M-E effects. Corrosion defects typically exhibit irregular geometries during the long-term corrosion process. To standardize integrity assessment, the American Society of Mechanical Engineers (ASME) approximates these defects as ellipsoidal or parabolic geometries [23]. The material API 5L X46 grade steel pipe was selected due to its widespread use in pipeline networks worldwide. The defect assessment of old pipelines is crucial for the integrity and operational safety of pipeline systems.

An elliptical shape was chosen to represent corrosion defects, as it more accurately reflects the typical geometry observed in real-world scenarios. The pipe was modeled with an outer diameter of 88.9 mm, a length of 1000 mm, and a wall thickness of 10 mm, as shown in Figure 1. In addition, a domain of computation (0.2 m × 0.2 m × 1 m) was developed to enclose the pipe model for the simulated NS4 solution. Two elliptical corrosion defects (100 mm length, 20 mm width, and varying depth) were developed on the outer surface of a pipe segment to model the M-E effect between defects. The defect depths are specified as 20%, 40%, 60%, and 80% of pipe wall thickness. According to ASME B31G standard [23], a corrosion depth reaching 80% of pipe wall thickness represents the critical threshold at which pipeline repair is required. The circumferential space between two corrosion defects is 5.96 mm. As depicted in Figure 1, the model also includes a soil domain surrounding the pipeline, with a solution conductivity of 0.096 S/m.

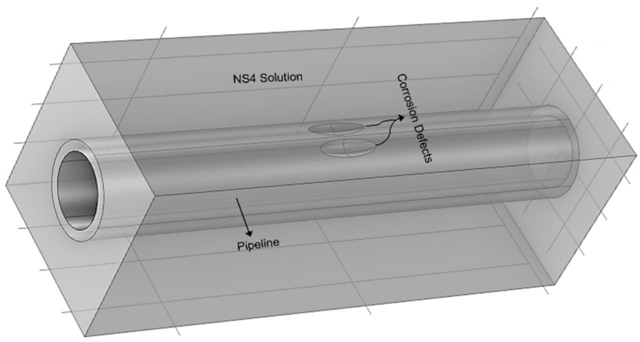

Fig. 1. 3D geometric model of steel pipe with elliptical corrosion defect exposed to NS4 soil solution.

The Parallel Direct Sparse Solver (PARDISO) was selected for the solution, with a relative tolerance of 0.02 to achieve convergence in nonlinear analysis. The boundary conditions were defined as follows: the steel/electrolyte interface was treated as a free boundary, while the outer boundaries were assumed to be electrically insulating. The surface of the corrosion defect was assumed to be the active anodic electrode. To simulate the mechanical constraints encountered in operational pipelines, the left end of the pipe was fully fixed, while the right end was subjected to hoop stress (σ_h) generated by operating pressure, as given by (1) [24]. A free tetrahedral mesh type was assigned to corrosion defects for mesh refinement, and a finer mesh was assigned for the remaining pipe sections. The maximum mesh sizes for the defect area and the remaining pipe body were 0.002 m and 0.08 m, respectively. A stress-based failure criterion was adopted to determine the onset of failure. Failure was assumed to occur when the maximum von Mises stress in the remaining pipe ligament reached the true ultimate tensile strength of the pipe material. In addition, the von Mises yield criterion was employed to evaluate the multiaxial stress distribution within the corroded pipe region:

$$\sigma_h = \frac{PD}{2t} \quad (1)$$

where P is the operating pressure, D is the outer diameter of the pipe, and t is the pipe wall thickness.

B. Mechanical Properties

The pipe material was modeled using the mechanical properties of API 5L X46 grade carbon steel, a commonly used material in oil and gas pipelines. The ultimate tensile stress (σ_{UTS}) of the pipe was 630 MPa at a strain of 0.1745. The modulus of elasticity (E) of the material was 207 GPa with a Poisson's ratio of 0.3. These parameters were assigned to the modeled pipe section. The mechanical properties of API 5L X46 steel pipe were determined using the nonlinear elastic-plastic model. The yield stress (σ_{ys}) of API 5L X46 steel pipe was 410 MPa [16] and the plastic stress followed a nonlinear isotropic hardening model:

$$\sigma_{yhard} = \sigma_{exp}(\varepsilon_{eff}) - \sigma_{ys} = \sigma_{exp}\left(\varepsilon_p + \frac{\sigma_e}{E}\right) - \sigma_{ys} \quad (2)$$

where σ_{yhard} represents the hardening function, σ_{exp} is the experimental stress function obtained from the stress-strain curve of X46 steel, ε_{eff} stands for the total effective strain, ε_p represents the plastic strain of steel, and σ_e is the effective stress.

C. Multiphysics Field Coupled M-E Effects

FE simulation was performed in three stages: (a) elasto-plastic stress analysis of the steel pipeline, examining mechanical behavior under loading conditions, (b) electrochemical modeling to determine potential distribution and current density patterns within the electrolyte solution and along the steel pipe surface, and (c) coupled M-E analysis to investigate the interaction between mechanical stresses and electrochemical processes at the solution-steel interface where corrosion defect is presented.

When mechanical damage or cathodic protection effects compromise a pipeline's anticorrosion coating, the underlying steel becomes exposed to corrosive solutions. This establishes a corrosion cell at the defect site, where the steel surface facilitates both anodic (iron dissolution) and cathodic (hydrogen evolution) reactions in near-neutral NS4 solution (pH 6.8), with the electrolyte completing the electron transfer pathway. This work assumes that only the exposed corrosion defect area participates actively in these electrochemical processes (Anodic reaction: $Fe \rightarrow Fe^{2+} + 2e^-$; Cathodic reaction: $H^+ + e^- \rightarrow H$), while the remaining coated pipeline surfaces remain electrochemically inert.

The anodic and cathodic reactions at the corrosion defect of the steel pipe in the NS4 solution are defined using kinetic equations [25]:

$$Anode\ Tafel = i_a = i_{0,a}\, exp\left(\frac{\eta_a}{b_a}\right) \quad (3)$$

$$Cathode\ Tafel = i_c = i_{0,c} exp\left(\frac{\eta_c}{b_c}\right) \quad (4)$$

$$Overpotential = \eta = \varphi - \varphi_{eq} \quad (5)$$

where i is the electrode current density reaction for anodic a and cathodic c , i_0 and b represents the exchange current density and Tafel slope, φ and φ_{eq} represent the electrode potential and the equilibrium electrode potential, respectively.

The Multiphysics coupled FE simulation provides the theoretical foundation for this work and has been established as an effective approach for investigating stress corrosion phenomena. This computational methodology has gained widespread adoption in corrosion science, enabling the investigation of complex scenarios that would be challenging or impractical to replicate through physical experimentation. The M-E effect on corrosion defects of pipelines integrates mechanical and electrochemical reactions.

Under the M-E effect, anodic and cathodic corrosion reactions on the electrode surface are influenced by the state of stress on the pipe wall and the corrosion defects. The anodic reaction influenced by the M-E effect was quantitatively measured in [12]:

$$\varphi_{a,eq} = \varphi^0_{a,eq} - \frac{\Delta P_m V_m}{zF} - \frac{TR}{zF}\ln\left(\frac{\upsilon\alpha}{N_0}\varepsilon_p + 1\right) \quad (6)$$

where $\varphi_{a,eq}$ represents the variation of the anodic equilibrium potential affected by the applied stress, $\varphi^0_{a,eq}$ is the standard equilibrium potential, ΔP represents excess pressure (P_a) equal to one-third of the uniaxial tensile stress, with its elastic limit ΔP_m calculated as one-third of the steel's yield strength. The key material parameters included molar volume (V_m = 7.13×10-^{6} m^3/mol), orientation factor (υ = 0.45), and dislocation coefficient (α = 1.67×10^{11} cm^{-2}). The initial density of dislocations before plastic deformation, N_0 , is 1×10^8 cm^{-2}. Finally, plastic strain, ε_p , is obtained through mechanical elasto-plastic simulation.

The M-E effect on the cathodic reaction was simplified to the cathodic exchange current density influenced by the von Mises stress:

$$i^s_{0,c} = i_{0,c} \times 10^{\frac{V_m \sigma_M}{6F(-b_c)}} \quad (7)$$

where $i^s_{0,c}$ is the exchange current density of the cathodic reaction under applied stress, $i_{0,c}$ denotes the exchange current density of cathodic reaction on the steel pipe in the absence of external stress or strain, and σ_M represents the von Mises stress, as calculated from FE simulation.

III. RESULTS

A. Model Validation

Before predicting the M-E effect on corrosion defects using the developed FE model, the simulation results were validated to ensure the model accuracy and reliability. The validation process determines the adequacy of the model's geometry, loading, boundary conditions, material properties, and meshing.

In this study, the model was validated by comparing the simulation results with the theoretical calculations. The theoretical calculations were examined from two critical aspects: the mechanical stress field with first principal stress calculations, and the electrochemical behavior, computing the anodic current density. The first principal stress was calculated in accordance with the ASME B31.4 [24] theoretical formula for hoop stress and axial stress in a pressurized cylindrical pipe, as given by (1). In addition, the anodic current density (i'_a) of stressed API 5L X46 steel electrode was calculated using [12]:

$$i'_a = i_{a,u}\, exp\left(\frac{\Delta P V_m}{RT}\right) \tag{8}$$

where $i_{a,u}$ is the anodic current density of an unstressed steel. The key input parameters incorporated into the multiphysics model comprised mechanical properties of the steel (true stress-strain curve, yield strength, and ultimate tensile strength), pipeline geometry (outer diameter and wall thickness), and electrochemical parameters governing corrosion kinetics (exchange current densities, equilibrium potentials, and Tafel slopes for both anodic and cathodic reactions).

Table I illustrates a comparison between the FE simulation predictions and analytical calculations of the first principal stress and anodic current density for an API 5L X46 steel pipeline immersed in NS4 solution under varying internal pressures. Excellent agreement was achieved in the mechanical domain, with the Relative Error (RE) for the first principal stress remaining below 1.8%. In the electrochemical domain, the anodic current density exhibited a moderately higher maximum RE of 5.55%, which is primarily attributable to the simplified porosity correction applied to the dynamically evolving corrosion product layer on the steel surface. Additionally, negative REs were consistently observed at low internal pressure levels for both the von Mises stress and anodic current density, reflecting the greater sensitivity of the FE model to subtle pressure variations compared to the corresponding analytical solutions.

TABLE I. COMPARISON OF THEORETICAL AND MODELING RESULTS UNDER DIFFERENT OPERATING PRESSURE

Internal pressure (MPa)		3	6	9	12
First principal stress (MPa)	Theoretical	13.34	26.67	40.01	53.34
	Simulation	13.19	26.21	39.59	53.01
	RE (%)	1.09	1.72	1.04	0.62
Anodic current density (μA/cm²)	Theoretical	3.56	3.63	3.70	3.77
	Simulation	3.65	3.69	3.51	3.56
	RE (%)	-2.60	-1.75	5.05	5.53

After validation, the distribution of the von Mises stress in the overall pipe wall for a corrosion defect with 8 mm depth and 0.3% tensile strain was analyzed, as shown in Figure 2. The results systematically examine the interplay between mechanical stress and electrochemical activity at the corrosion defect. It can be seen that the steel pipe exhibits high stress at corrosion defects, highlighted by a dark red color.

B. Von Mises Stress, Corrosion Potential, and Net Current Density Distributions

The distributions of corrosion potential and von Mises stress at the pipe corrosion defect with 8 mm fixed depth and various tensile strain conditions are illustrated in Figure 3. The von Mises stress (MPa) and corrosion potential (V and SCE) are also illustrated as colour legends on the right and left sides in Figure 3, where significantly higher stress concentration is observed at the defect area compared to the pipe wall at tensile strains of 1% and 2%. In addition, the solution potential field remains uniform. As the tensile strain increased to 0.4%, stress also increased gradually, leading to plastic deformation, as represented by the dark red colour at the defect area of the pipeline. This indicates that high tensile strain leads to a more negative potential and a corresponding increase in local stress.

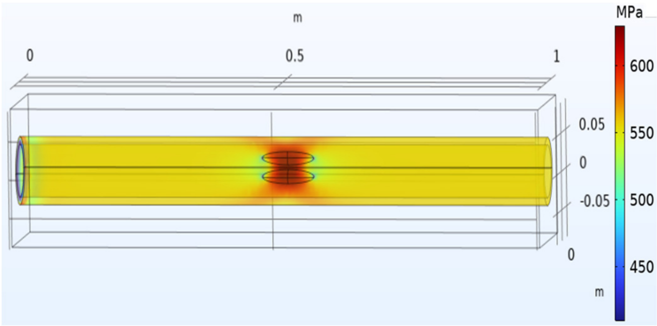

Fig. 2. Distribution of stress in the pipe inner wall for a corrosion defect depth of 8 mm and 0.3% tensile strain.

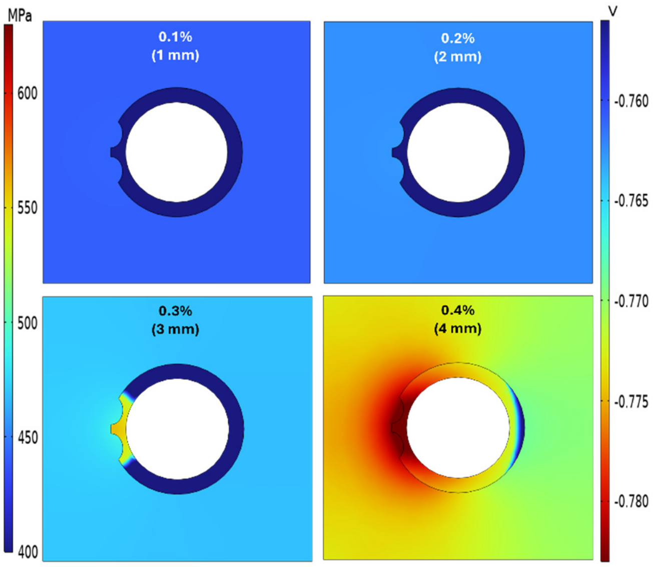

Fig. 3. Von Mises stress and corrosion potential distributions at a corrosion defect with a depth of 8 mm under varying tensile strains.

Figure 4 displays the von Mises stress and corrosion potential distributions at the defect area with 0.4% tensile strain and varying defect depths. The results indicate that shallow corrosion defects of 20% and 40% of pipe wall thickness, corresponding to depths of 2 mm and 4 mm, do not significantly alter the potential field within the NS4 solution and remain below the yield strength of the material (806 MPa).

However, as defect depth increased further from 60% to 80% of pipe wall thickness, an increase in the von Mises stress was also observed at the corrosion defect. Therefore, corrosion potential distribution appeared uneven, with a notably higher potential at the corrosion defect compared to other areas of the pipe in the NS4 solution.

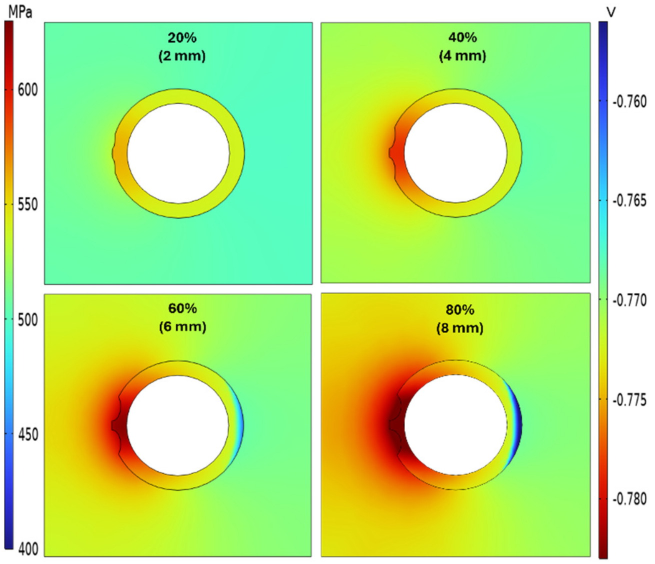

Fig. 4. Von Mises stress and corrosion potential distributions at a corrosion defect with 0.3% tensile strain and varying defect depths.

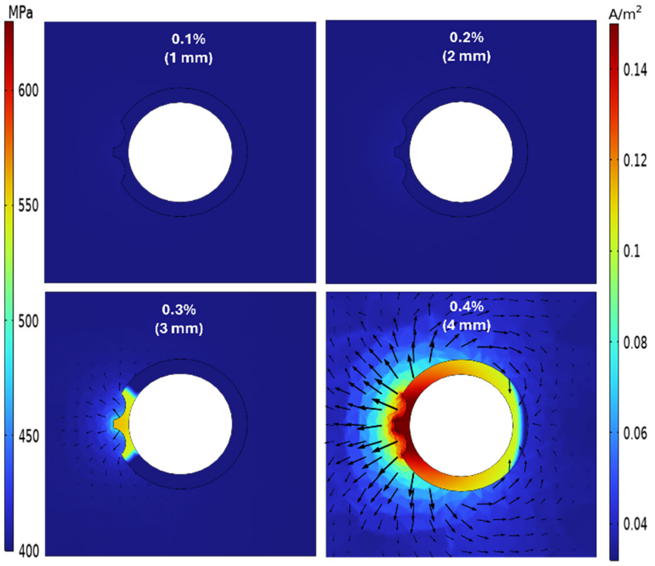

Fig. 5. Net current density and von Mises stress distributions at a corrosion defect with 8 mm depth and varying tensile strains.

Figure 5 depicts the corrosion potential, distribution of net current density, and von Mises stress at the pipe corrosion defect with 8 mm depth and various tensile strains. Stress concentration at the defect area showed a nearly symmetrical distribution, with a peak at the defect center. As tensile strain increased from 0.1% to 0.4%, the stress also increased correspondingly. The electrostatic current density remained low in the NS4 solution until tensile strain reached 0.3%, indicating that the entire pipeline was operating with deformation within the elastic range. As tensile stress increased from 0.3% to 0.4%, the stress at the defect exceeded the yield strength of X100 steel, leading to a shift from elastic to plastic deformation.

Figure 6 illustrates von Mises stress and net current density distributions at a pipe corrosion defect with 0.4% tensile strain and various defect depths. High stress concentration was observed at the corrosion defect when the defect depth exceeded 20% of the pipe wall thickness. It is observed that the entire pipeline entered into the plastic region even at a small defect depth 20% of the pipe wall thickness. Additionally, in Figure 6, a pronounced net current flow in the NS4 solution is noted, as highlighted by vectors directed from the defect center outward.

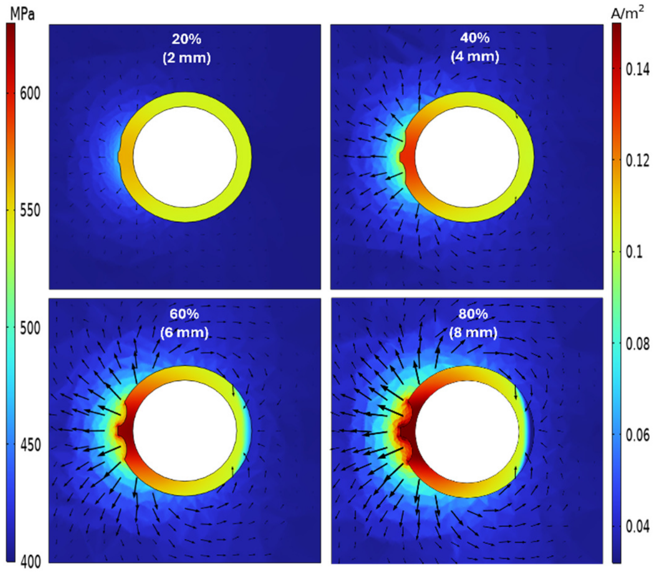

Fig. 6. Von Mises stress and net current density distributions at a corrosion defect with 0.4% tensile strain and varying defect depths.

IV. DISCUSSION

The simulation results demonstrate that an increase in corrosion defect size, internal pressure, pipe service time, and tensile strain leads to stress concentrations in the pipeline wall that exceed the safe limits of the material, although their influence on stress distribution differs significantly. Since mechanical stress influences the electrochemical potential distribution of steel, corrosion at the defect is considered to be composed of a series of local galvanic cells. In these cells, regions with high stress, such as the defect center, act as anodic sites, while the lower stress regions, such as the defect sides, serve as cathodic areas. The accelerated hydrogen evolution was captured in the model by an increased cathodic exchange current density.

The increase in defect depth is attributed to higher stress concentration in deeper regions due to the M-E effect. It is observed that increasing defect depth leads to a more concentrated stress at the defect center. This makes the corrosion growth rate more pronounced in the depth direction. Moreover, when tensile strain, induced by soil movement or ground deformation, is applied to a pipe model with a corrosion defect, the axial force in any cross-section remains constant (according to the equilibrium principle). However, this stress distribution becomes non-uniform due to geometric variations, such as lower stress at the corrosion defect sides and higher stress concentration at the defect center. As hoop stress in pressurized pipelines is typically twice the longitudinal stress, the first principal stress acts primarily in the circumferential direction. Consequently, stress corrosion cracks tend to propagate longitudinally, perpendicular to the dominant hoop stress, a pattern observed in field inspections of oil and gas pipelines.

V. CONCLUSION

The study identified critical factors influencing stress corrosion driven by Mechano-Electrochemical (M-E) effects. A Three-Dimensional (3D) Finite Element (FE) model was utilized to examine the influence of key factors, including defect geometry, operational parameters, ground movement (tensile strain), and environmental conditions (NS4 solution). The FE model was developed to simulate stress corrosion, incorporating M-E effects at double corrosion defects in a carbon steel pipeline (API 5L X46). The results revealed that under elastic deformation (0.1-0.2% tensile strain), corrosion potential remains uniform, but plastic deformation (0.4% tensile strain at 8 mm defect depth) induces a negative potential shift, driving localized corrosion at defect centers. The FE analysis results show that the simulation is capable of predicting the failure of corroded oil and gas pipelines. Even when pipelines operate within design limits, localized corrosion defects in aggressive environments can still trigger catastrophic failure. Within these defects, a macroscopic corrosion cell is established, with the defect center acting as the anode and undergoing accelerated dissolution, while the adjacent defect edges are cathodically protected. The results also reveal that corrosion propagates preferentially downward along the defect centerline, leading to continuous deepening and thinning of the remaining ligament until ultimate failure occurs.

ACKNOWLEDGMENT

The authors would like to thank Universiti Teknologi PETRONAS, Malaysia, for providing the opportunity to conduct research under grant number 015LB0-151 for the project "Integrated Ensemble Learning-Assisted Prediction of Stress Corrosion in Carbon Steel Pipelines".

REFERENCES

[1] Y. Guang, W. Wang, H. Song, H. Mi, J. Tang, and Z. Zhao, "Prediction of External Corrosion Rate for Buried Oil and Gas Pipelines: A Novel Deep Learning Method with DNN and Attention Mechanism," *International Journal of Pressure Vessels and Piping*, vol. 209, Jun. 2024, Art. no. 105218, https://doi.org/10.1016/j.ijpvp.2024.105218.

[2] U. Sarwar *et al.*, "Enhancing Pipeline Integrity: A Comprehensive Review of Deep Learning-Enabled Finite Element Analysis for Stress Corrosion Cracking Prediction," *Engineering Applications of Computational Fluid Mechanics*, vol. 18, no. 1, Dec. 2024, Art. no. 2302906, https://doi.org/10.1080/19942060.2024.2302906.

[3] A. A. Soomro, O. K. Siddiqui, A. Shams, and B. Almomani, "Machine Learning Applications in Nuclear Power Plant Piping Inspection: A Review of Methods, Data, and Future Trends," *Annals of Nuclear Energy*, vol. 225, Jan. 2026, Art. no. 111760, https://doi.org/10.1016/j.anucene.2025.111760.

[4] B. Zhang, H. Lei, X. Hu, and C.-Q. Li, "Time-Dependent Reliability of Corroded Mild Steel Pipes by Different Failure Modes," *International Journal of Pressure Vessels and Piping*, vol. 207, Feb. 2024, Art. no. 105100, https://doi.org/10.1016/j.ijpvp.2023.105100.

[5] A. A. Soomro *et al.*, "A Review on Bayesian Modeling Approach to Quantify Failure Risk Assessment of Oil and Gas Pipelines Due to Corrosion," *International Journal of Pressure Vessels and Piping*, vol. 200, Dec. 2022, Art. no. 104841, https://doi.org/10.1016/j.ijpvp.2022.104841.

[6] Z. Zhao, M. N. Akhtar, E. A. Bakar, and N. B. Abdul Razak, "A Review on Corrosion Modelling for Submarine Pipeline," *Ain Shams Engineering Journal*, vol. 16, no. 7, Jul. 2025, Art. no. 103411, https://doi.org/10.1016/j.asej.2025.103411.

[7] W. Wang, Y. Guang, W. Liu, K. Shen, M. Huffman, and Q. Wang, "Experimental Investigation of Stress Corrosion on Supercritical CO2 Transportation Pipelines Against Leakage for CCUS Applications," *Energy Reports*, vol. 9, pp. 266–276, Dec. 2023, https://doi.org/10.1016/j.egyr.2022.11.179.

[8] S.-M. Filip, E. Avrigean, and A.-M. Pascu, "Damage to Natural Gas Distribution Steel Pipelines Caused by Rigid Bodies resulting from the Excavation of Laying Trenches," *Engineering, Technology & Applied Science Research*, vol. 14, no. 1, pp. 12984–12987, Feb. 2024, https://doi.org/10.48084/etasr.6716.

[9] R. Pourazizi, M. A. Mohtadi-Bonab, and J. A. Szpunar, "Investigation of Different Failure Modes in Oil and Natural Gas Pipeline Steels," *Engineering Failure Analysis*, vol. 109, Jan. 2020, Art. no. 104400, https://doi.org/10.1016/j.engfailanal.2020.104400.

[10] P. Jiang *et al.*, "Investigation into the Mechano-Electrochemical Interaction of Internal and External Corrosion Defects on Pipe Surfaces," *International Journal of Pressure Vessels and Piping*, vol. 207, Feb. 2024, Art. no. 105098, https://doi.org/10.1016/j.ijpvp.2023.105098.

[11] Z. Zhang, J. Zhang, and M. Ding, "Effect of External Wall Defect Growth on Internal Wall Corrosion of Oil Pipelines Under Mechano-Electrochemical Interaction," *The Canadian Journal of Chemical Engineering*, vol. 101, no. 3, pp. 1398–1409, Mar. 2023, https://doi.org/10.1002/cjce.24577.

[12] E. M. Gutman, *Mechanochemistry of Materials*. Cambridge, MA, USA: Cambridge International Science Publishing, 1998.

[13] Y. Wang, J. A. Wharton, and R. A. Shenoi, "Mechano-Electrochemical Modelling of Corroded Steel Structures," *Engineering Structures*, vol. 128, pp. 1–14, Dec. 2016, https://doi.org/10.1016/j.engstruct.2016.09.015.

[14] L. Y. Xu and Y. F. Cheng, "Development of a Finite Element Model for Simulation and Prediction of Mechanoelectrochemical Effect of Pipeline Corrosion," *Corrosion Science*, vol. 73, pp. 150–160, Aug. 2013, https://doi.org/10.1016/j.corsci.2013.04.004.

[15] L. Xu and Y. F. Cheng, "A Finite Element Based Model for Prediction of Corrosion Defect Growth on Pipelines," *International Journal of Pressure Vessels and Piping*, vol. 153, pp. 70–79, Jun. 2017, https://doi.org/10.1016/j.ijpvp.2017.05.002.

[16] J. Sun and Y. F. Cheng, "Modelling of Mechano-Electrochemical Interaction of Multiple Longitudinally Aligned Corrosion Defects on Oil/Gas Pipelines," *Engineering Structures*, vol. 190, pp. 9–19, Jul. 2019, https://doi.org/10.1016/j.engstruct.2019.04.010.

[17] Z.-W. Zhang, J.-C. Wang, J.-H. Zhang, and Y. F. Cheng, "Modeling of the Mechano-Electrochemical Effect at Corrosion Defect with Varied Inclinations on Oil/Gas Pipelines," *Petroleum Science*, vol. 18, no. 5, pp. 1520–1529, Oct. 2021, https://doi.org/10.1016/j.petsci.2021.08.012.

[18] Y. Shuai *et al.*, "Assessment by Finite Element Modelling of the Mechano-Electrochemical Interaction at Corrosion Defect on Elbows of Oil/Gas Pipelines," *Ocean Engineering*, vol. 234, Aug. 2021, Art. no. 109228, https://doi.org/10.1016/j.oceaneng.2021.109228.

[19] G. Qin, Y. Huang, Y. Wang, and Y. F. Cheng, "Pipeline Condition Assessment and Finite Element Modeling of Mechano-Electrochemical Interaction Between Corrosion Defects with Varied Orientations on

Pipelines," *Tunnelling and Underground Space Technology*, vol. 136, Jun. 2023, Art. no. 105101, https://doi.org/10.1016/j.tust.2023.105101.

[20] G. Qin, Y. F. Cheng, and P. Zhang, "Finite Element Modeling of Corrosion Defect Growth and Failure Pressure Prediction of Pipelines," *International Journal of Pressure Vessels and Piping*, vol. 194, Dec. 2021, Art. no. 104509, https://doi.org/10.1016/j.ijpvp.2021.104509.

[21] H. Liu, Y. Ma, Y. Du, M. Li, and Y. Shen, "A Numerical Analysis of the Mechano-Electrochemical Effects on Localised Corrosion in Pipelines Using a Multi-Physical Field Coupling Approach," *Ocean Engineering*, vol. 310, Oct. 2024, Art. no. 118522, https://doi.org/10.1016/j.oceaneng.2024.118522.

[22] M. Subasic, C. F. O. Dahlberg, and P. Efsing, "An Elastoplastic Formulation for Mechanical-Electrochemical Corrosion Damage Under Cyclic Loading," *Corrosion Science*, vol. 255, Oct. 2025, Art. no. 113145, https://doi.org/10.1016/j.corsci.2025.113145.

[23] Manual for Determining the Remaining Strength of Corroded Pipelines, ASME B31G-2012, New York City, NY, USA, Oct. 2012.

[24] Pipeline Transportation Systems for Liquids and Slurries, ASME-B31.4, New York City, NY, USA, Dec. 2022.

[25] Z. Zhang, X. Ni, and Y. F. Cheng, "Assessment by Finite Element Modelling of the Mechano-Electrochemical Interaction at Double-Ellipsoidal Corrosion Defect with Varied Inclinations on Pipelines," *Construction and Building Materials*, vol. 260, Nov. 2020, Art. no. 120459, https://doi.org/10.1016/j.conbuildmat.2020.120459.